

Testing $WW\gamma$ vertex in radiative muon decay

Anirban Karan^{*} and Rahul Sinha[†]

*The Institute of Mathematical Sciences, Taramani, Chennai 600113, India and
Homi Bhabha National Institute, BARC Training School Complex, Anushaktinagar, Mumbai 400094, India*

Rusa Mandal[‡]

IFIC, Universitat de València-CSIC, Apt. Correus 22085, E-46071 València, Spain

(Dated: February 14, 2019)

Large numbers of muons will be produced at facilities developed to probe lepton flavor violating process $\mu \rightarrow e\gamma$. We show that by constructing a suitable asymmetry, radiative muon decay $\mu \rightarrow e\gamma\nu_\mu\bar{\nu}_e$ can also be used to test the $WW\gamma$ vertex at such facilities. The process has two missing neutrinos in the final state and on integrating their momenta, the partial differential decay rate shows no radiation-amplitude-zero. We establish, however, that an easily separable part of the normalized differential decay rate, odd under the exchange of photon and electron energies, does have a zero in the case of standard model (SM). This *new type of zero* has hitherto not been studied in literature. A suitably constructed asymmetry using this fact, enables a sensitive probe for the $WW\gamma$ vertex beyond the SM. With a simplistic analysis, we find that the C and P conserving dimension four $WW\gamma$ vertex can be probed at $\mathcal{O}(10^{-2})$ with satisfactory significance level.

I. INTRODUCTION

The $SU(2)_L \otimes U(1)_Y$ theory of electroweak interactions has been tested extensively in last few decades and there is no doubt that it is the correct theory at least up to a TeV scale. This conviction is largely based on the precision measurements at LEP and the consistency of top and Higgs boson masses which could be predicted taking radiative corrections into account. The gauge boson and Higgs boson self interactions are, however, not as well probed either by direct measurement or by radiative corrections and it is possible that some deviations from the standard Model (SM) loop level values might still be seen. To ascertain the validity of SM it is critical that the $WW\gamma$ vertex, which is predicted uniquely in SM, be probed to an accuracy consistent with loop level corrections to it. Several experiments [1–8] have measured parameters that probe the $WW\gamma$ and WWZ vertex, but the accuracy achieved is still insufficient to probe one loop corrections to it within the SM.

In this paper, we have investigated how the C and P conserving dimension four $WW\gamma$ operator can be probed experimentally using radiative muon decays. The vertex factor for this operator is usually denoted by κ_γ and is uniquely predicted in the SM. At tree level $\kappa_\gamma = 1$ in the SM and the absolute value of the one loop corrections to the tree level values of κ_γ is restricted to be less than 1.5×10^{-2} [9]. However, the current global average $\kappa_\gamma = 0.982 \pm 0.042$ [10] has too large an uncertainty to probe the SM up to one loop accuracy. Of the experimentally measured values of κ_γ , only ATLAS and CMS collaborations use the data for real on-shell photon emis-

sion in hadron colliders [1, 2], probing the true magnetic moment of the W -boson.

One can expect κ_γ to deviate from its SM value by only a few percent, hence, we must choose the mode to be studied very carefully. Radiative muon decay $\mu \rightarrow e\gamma\nu_\mu\bar{\nu}_e$ is a promising mode to measure the true magnetic moment (due to real photon in the final state) of the W -boson in this regard. At first sight the measurement of W -boson gauge coupling using low energy decay process may seem impossible, since the effect is suppressed by two powers of the W -boson mass. The process has two missing neutrinos in the final state and on integrating their momenta the partial differential decay rate shows no radiation-amplitude zero [11]. Moreover, the differential decay rate does not show enough sensitivity to a deviation of the $WW\gamma$ vertex from that of the SM. We show, however, that an easily separable part the normalized differential decay rate (odd under the exchange of photon and electron energies) does have a zero in the case of SM. The vanishing of the odd contribution under the exchange of final state electron and photon energies in the decay rate is a *new type of zero*, hitherto not been studied in literature. A suitably constructed asymmetry using this fact enables adequate sensitivity to probe the $WW\gamma$ vertex beyond the SM. We consider a very restricted part of the phase space where the asymmetry is larger than statistical errors for our study. Large number of muons are expected to be produced for COMET [12], MEG [13] and Mu2e [14] collaborations to probe lepton flavor violating processes like $\mu \rightarrow e\gamma$. The radiative muon decay $\mu \rightarrow e\gamma\nu_\mu\bar{\nu}_e$ [15] discussed in this paper is the dominant background process for this case. The large sample of $\mu \rightarrow e\gamma\nu_\mu\bar{\nu}_e$ produced at such facilities make them an ideal environment to probe $WW\gamma$ vertex, with reduced statistical uncertainty, as discussed in this paper. In a simulation using $\eta_\gamma \equiv \kappa_\gamma - 1 = 0.01$, we find that the asymmetry constructed by us, can probe this η_γ value with a 3.9σ significance.

^{*} kanirban@imsc.res.in

[†] sinha@imsc.res.in

[‡] Rusa.Mandal@ific.uv.es

The rest of the paper is organized as follows. In Sec. II we briefly discuss the decay kinematics and relevant expressions for decay rate. These results are used to construct the observables in Sec. III, where we also explain why a zero in odd amplitude is expected. Section. IV deals with the numerical analysis to probe the $WW\gamma$ vertex and finally we conclude in Sec. V.

II. THEORETICAL FRAMEWORK

In this section we briefly discuss the theoretical set up for the radiative muon decay. The radiative muon decay proceeds through three Feynman diagrams, shown in Fig. 1, where the photon in the final state can either arise from any of the initial and final state leptons or the W boson in the propagator. The later process is of our particular interest. We define the four momenta of

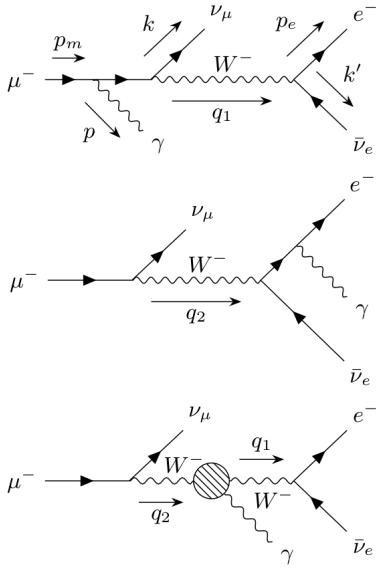


FIG. 1. Feynman diagrams for radiative muon decay.

incoming μ^- , outgoing e^- , γ , ν_μ , $\bar{\nu}_e$ as p_m , p_e , p , k and k' , respectively, and the masses of muon, electron and W -boson are denoted by m_μ , m_e and m_W , respectively. The amplitudes corresponding to these three diagrams (from top to bottom), labelled with subscript 1 to 3, can be expressed as

$$i\mathcal{M}_1 = \left(\frac{-ieg^2}{8}\right)\bar{u}(p_e)\gamma_\beta(1-\gamma_5)v(k')\left[\frac{g^{\alpha\beta} - \frac{q_1^\alpha q_1^\beta}{m_W^2}}{q_1^2 - m_W^2}\right] \\ \times \bar{u}(k)\gamma_\alpha(1-\gamma_5)\left[\frac{1}{\not{p}_m - \not{p} - m_\mu}\right]\gamma_\delta u(p_m)\epsilon^{*\delta}, \quad (1)$$

$$i\mathcal{M}_2 = \left(\frac{-ieg^2}{8}\right)\bar{u}(k)\gamma_\alpha(1-\gamma_5)u(p_m)\left[\frac{g^{\alpha\beta} - \frac{q_2^\alpha q_2^\beta}{m_W^2}}{q_2^2 - m_W^2}\right]$$

$$\times \bar{u}(p_e)\gamma_\delta\left[\frac{1}{\not{p}_e + \not{p} - m_e}\right]\gamma_\beta(1-\gamma_5)v(k')\epsilon^{*\delta}, \quad (2)$$

$$i\mathcal{M}_3 = \left(\frac{-ieg^2}{8}\right)\bar{u}(k)\gamma_\alpha(1-\gamma_5)u(p_m)\left[\frac{g^{\alpha\rho} - \frac{q_2^\alpha q_2^\rho}{m_W^2}}{q_2^2 - m_W^2}\right] \\ \times \left[\frac{g^{\sigma\beta} - \frac{q_1^\sigma q_1^\beta}{m_W^2}}{q_1^2 - m_W^2}\right]\bar{u}(p_e)\gamma_\beta(1-\gamma_5)v(k') \\ \times \Gamma_{\rho\sigma\delta}(q_2, q_1, p)\epsilon^{*\delta}, \quad (3)$$

where e and g are the charge of positron and weak coupling constant, respectively; $q_1^\mu = p_e^\mu + k'^\mu$ and $q_2^\mu = p_m^\mu - k^\mu$. In Eq. (3), $\Gamma_{\rho\sigma\delta}(q_2, q_1, p)$ denotes the effective triple gauge boson vertex for electroweak interaction as shown in Fig. 2.

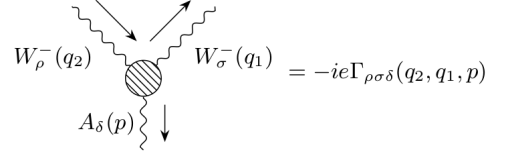


FIG. 2. Feynman rule for effective $WW\gamma$ vertex.

The most general couplings of W to the neutral gauge bosons γ and Z can be described by the following effective Lagrangian [16],

$$\mathcal{L}_{eff}^V = -ig_V[g_1^V(W_{\mu\nu}^\dagger W^\mu - W^{\dagger\mu}W_{\mu\nu})V^\nu \\ + \kappa_V W_\mu^\dagger W_\nu V^{\mu\nu} + \frac{\lambda_V}{m_W^2} W_\lambda^\dagger W_\nu^\mu V^{\nu\lambda} \\ + if_4^V W_\mu^\dagger W_\nu(\partial^\mu V^\nu + \partial^\nu V^\mu) \\ - if_5^V \epsilon^{\mu\nu\rho\sigma}(W_\mu^\dagger \overleftrightarrow{\partial}_\rho W_\nu)V_\sigma \\ + \tilde{\kappa}_V W_\mu^\dagger W_\nu \tilde{V}^{\mu\nu} + \frac{\tilde{\lambda}_V}{m_W^2} W_\lambda^\dagger W_\nu^\mu \tilde{V}^{\nu\lambda}]. \quad (4)$$

Here, V corresponds to γ or Z , $g_\gamma = e$ and $g_Z = e \cot \theta_W$ where θ_W is the Weinberg angle. $W_{\mu\nu} = \partial_\mu W_\nu - \partial_\nu W_\mu$, $V_{\mu\nu} = \partial_\mu V_\nu - \partial_\nu V_\mu$, $\tilde{V}_{\mu\nu} = \frac{1}{2}\epsilon_{\mu\nu\rho\sigma}V^{\rho\sigma}$, $(A\overleftrightarrow{\partial}_\mu B) = A(\partial_\mu B) - (\partial_\mu A)B$ and Bjorken-Drell metric is taken as $\epsilon_{0123} = -\epsilon^{0123} = +1$. In the SM, at tree level, $g_1^V = \kappa_V = 1$ and all other coupling parameters are zero.

In the case of radiative muon decay, the vertex with W boson pair and a photon field is involved where among the seven coupling parameters, f_4^γ , $\tilde{\kappa}_\gamma$ and $\tilde{\lambda}_\gamma$ denote the coupling strengths of CP violating interactions in the Lagrangian (in Eq. (4)) and are constrained to be less than $\sim (10^{-4})$ [17] due to the measurements of neutron electric dipole moment in case of direct CP violation. Due to the CP violating nature of these couplings, deviations from the SM contributions are proportional to square of these couplings and thus are highly suppressed, as compared to CP -conserving contributions. Hence, we neglect the

CP violating parameters for the rest of the discussion of the paper. The demand of C and P to be conserved separately in the Lagrangian allows us to choose vanishing f_5^γ . It is obvious that the muon radiative decay will not be sensitive to the dimension six-operator involving λ_γ , due to an additional m_W^2 suppression. The measurement of λ_γ is possible only at high energy colliders. Hence, we can safely neglect the deviation of λ_γ from its SM value of zero. Furthermore, the value of the coupling g_1^γ is fixed to be unity due to electromagnetic gauge invariance. Thus, in momentum space the $WW\gamma$ vertex can be expressed as

$$\Gamma_{\rho\sigma\delta}(q_2, q_1, p) = g_{\rho\sigma}(q_2 + q_1)_\delta + g_{\sigma\delta}(p - q_1)_\rho - g_{\delta\rho}(p + q_2)_\sigma + \eta_\gamma(p_\rho g_{\sigma\delta} - p_\sigma g_{\rho\delta}), \quad (5)$$

where $\eta_\gamma \equiv \kappa_\gamma - 1$ and q_2, q_1, p are the four momenta of incoming W^- , outgoing W^- and outgoing photon respectively, as depicted in Fig. 2.

It is apparent from Fig. 1 and Eqs. (1)-(3), that amplitude (\mathcal{M}_3) containing effective vertex $\Gamma_{\rho\sigma\delta}$ is $1/m_W^2$ suppressed compared to the other two contributions \mathcal{M}_1 and \mathcal{M}_2 . Hence, within the SM, the first two Feynman-diagrams in Fig. 1 are sufficient to study the process. On the other hand only the third diagram is sensitive to η_γ . Thus, in order to retain sensitivity to η_γ in $\Gamma_{\rho\sigma\delta}$, it is necessary and sufficient to keep contributions up to $\mathcal{O}(1/m_W^4)$, in the amplitudes. To achieve this we expand the W boson propagator in the power series of (q_j^2/m_W^2) as

$$-i \left[\frac{g^{\alpha\beta} - \frac{q_j^\alpha q_j^\beta}{m_W^2}}{q_j^2 - m_W^2} \right] \approx \frac{i}{m_W^2} \left[g^{\alpha\beta} + \frac{q_j^2}{m_W^2} \left(g^{\alpha\beta} - \frac{q_j^\alpha q_j^\beta}{q_j^2} \right) \right]. \quad (6)$$

The total amplitude can be expressed as $\mathcal{M} = \mathcal{M}_1 + \mathcal{M}_2 + \mathcal{M}_3$ and we calculate differential cross section keeping all the amplitudes up to $\mathcal{O}(1/m_W^4)$. Since the neutrinos ν_μ and $\bar{\nu}_e$ cannot be observed we integrate the ν_μ and $\bar{\nu}_e$ momenta, and define the $\nu_\mu \bar{\nu}_e$ invariant momentum as q . As the decay now looks like a 3-body decay it is meaningful to define effective Mandelstam like variable constructed from the invariant momentum square of $e^- \nu_\mu \bar{\nu}_e$ system as t and that of $\gamma \nu_\mu \bar{\nu}_e$ system as u . Hence, $(p_e + q)^2 = t$ and $(p_\gamma + q)^2 = u$. Notice that, q^2 is not a constant for our decay. It is, however, much more convenient to define normalized parameters

$$\begin{aligned} x_p &= \frac{t + u}{2(q^2 + m_\mu^2)}, \\ y_p &= \frac{t - u}{2(q^2 + m_\mu^2)}, \\ q_p^2 &= \frac{q^2}{(q^2 + m_\mu^2)}, \end{aligned} \quad (7)$$

which can be written in terms of the observable quantities, the photon energy E_γ , the electron energy E_e and

the angle between the electron and photon θ as follows.

$$x_p = \frac{m_\mu(m_\mu - E_e - E_\gamma)}{2[m_\mu^2 - E_\gamma m_\mu - E_e m_\mu + E_e E_\gamma(1 - \cos \theta)]}, \quad (8)$$

$$y_p = \frac{m_\mu(E_e - E_\gamma)}{2[m_\mu^2 - E_\gamma m_\mu - E_e m_\mu + E_e E_\gamma(1 - \cos \theta)]}, \quad (9)$$

$$q_p^2 = \frac{m_\mu^2 - 2E_\gamma m_\mu - 2E_e m_\mu + 2E_e E_\gamma(1 - \cos \theta)}{2[m_\mu^2 - E_\gamma m_\mu - E_e m_\mu + E_e E_\gamma(1 - \cos \theta)]}. \quad (10)$$

The parameters of interest for the derivation, x_p , y_p and q_p^2 can easily be inverted in terms of the observables E_e , E_γ and $\cos \theta$ as,

$$E_e = \frac{m_\mu}{2} \left(\frac{1 - q_p^2 - x_p + y_p}{1 - q_p^2} \right), \quad (11)$$

$$E_\gamma = \frac{m_\mu}{2} \left(\frac{1 - q_p^2 - x_p - y_p}{1 - q_p^2} \right), \quad (12)$$

$$\cos \theta = \frac{(q_p^2 - x_p)^2 + 2x_p - y_p^2 - 1}{(1 - q_p^2 - x_p)^2 - y_p^2}. \quad (13)$$

We notice that replacing y_p by $-y_p$ while keeping q_p^2 and x_p unchanged actually results in swapping the energies of photon and electron keeping the angle between them unaltered. This feature will play a very crucial role in defining the observable asymmetry in Sec. III.

We have ignored the electron mass, m_e , starting from Eq. (7) as it results in significant simplification of analytic expressions. It is of course well-known that neglecting the electron mass results in the persistence of wrong helicity right-handed electron [18, 19] in this decay as a result of inner bremsstrahlung from the electron (see second diagram of Fig. 1). The results are in obvious disagreement depending on whether m_e is retained or not. We will therefore very carefully consider the issue of electron mass to justify the neglect of m_e for our limited purpose of extracting η_γ , while acknowledging that m_e should not be ignored in general. In order to retain maximum sensitivity to η_γ the kinematic domain is chosen to minimize the soft photon and collinear singularity contributions; the effect of m_e is found to be insignificant in the kinematic domain sensitive to η_γ . Our calculations have been verified retaining m_e throughout. Critical expressions including m_e contributions are presented in Appendix A for clarity. Expressions for x_p and y_p are modified to accommodate effects of m_e , while retaining an *apparent exchange symmetry* between E_γ and E_e under the newly defined variables x_n and y_n in Eq. (A6).

We consider only the normalized differential decay rate $\bar{\Gamma}(x_p, y_p, q_p^2)$ obtained after integrating the ν_μ and $\bar{\nu}_e$ momenta which is defined as

$$\bar{\Gamma}(x_p, y_p, q_p^2) = \frac{1}{\Gamma_\mu} \cdot \frac{d^3\Gamma}{dq_p^2 dx_p dy_p}, \quad (14)$$

where, Γ_μ is the total decay width of muon. In terms of these new normalized variables, the phase space for this

process is bounded by three surfaces: $q_p^2 = 0$, $x_p = 1/2$ and $(q_p^4 - q_p^2 + x_p^2 - y_p^2) = 0$. It is easily seen from Eq. (13), the plane $x_p = 1/2$ corresponds to $\theta = 0^\circ$ and the curved surface $(q_p^4 - q_p^2 + x_p^2 - y_p^2) = 0$ signifies $\theta = 180^\circ$. The physical region in q_p^2 , x_p and y_p parameter space is given by,

$$\begin{aligned} q_p \sqrt{1 - q_p^2} &\leq x_p \leq \frac{1}{2}, \\ |y_p| &\leq \left(\frac{1}{2} - q_p^2\right), \\ (q_p^4 - q_p^2 + x_p^2 - y_p^2) &\geq 0, \\ 0 &\leq q_p^2 \leq \frac{1}{2}. \end{aligned} \quad (15)$$

Form Eq. (7) and Eq. (15), it is clear that both q_p^2 and x_p are positive valued functions whereas y_p can have a positive value or a negative value and the physical region allows y_p to have a range symmetric about $y_p = 0$. So, if (x_p, y_p, q_p^2) be a point inside physical region, $(x_p, -y_p, q_p^2)$ will also lie inside the allowed region. This motivates us to investigate the properties of odd and even part of $\bar{\Gamma}(x_p, y_p, q_p^2)$ under the variable y_p . In the next section (Sec. III) we construct such an observable as the ratio of odd part in y_p divided by even part in y_p of $\bar{\Gamma}(x_p, y_p, q_p^2)$ and demonstrate its heightened sensitivity to η_γ .

III. OBSERVABLE AND ASYMMETRY

The ‘odd’ and ‘even’ part $\bar{\Gamma}_o(x_p, y_p, q_p^2)$ and $\bar{\Gamma}_e(x_p, y_p, q_p^2)$, respectively, of the normalized differential decay rate (Eq. (14)) with respect to y_p are defined as

$$\begin{aligned} \bar{\Gamma}_o(x_p, y_p, q_p^2) &= \frac{1}{2} [\bar{\Gamma}(x_p, y_p, q_p^2) - \bar{\Gamma}(x_p, -y_p, q_p^2)] \\ &\approx F_o(x_p, y_p, q_p^2) + \eta_\gamma G_o(x_p, y_p, q_p^2), \end{aligned} \quad (16)$$

$$\begin{aligned} \bar{\Gamma}_e(x_p, y_p, q_p^2) &= \frac{1}{2} [\bar{\Gamma}(x_p, y_p, q_p^2) + \bar{\Gamma}(x_p, -y_p, q_p^2)] \\ &\approx F_e(x_p, y_p, q_p^2) + \eta_\gamma G_e(x_p, y_p, q_p^2), \end{aligned} \quad (17)$$

where the small η_γ^2 terms are ignored.

As we have obtained $\bar{\Gamma}(x_p, y_p, q_p^2)$ by integrating a positive valued function $|\mathcal{M}|^2$, it is obvious that both $\bar{\Gamma}(x_p, y_p, q_p^2)$ and $\bar{\Gamma}(x_p, -y_p, q_p^2)$ will be positive. Hence, $\bar{\Gamma}_e(x_p, y_p, q_p^2)$, which is proportional to the sum of $\bar{\Gamma}(x_p, y_p, q_p^2)$ and $\bar{\Gamma}(x_p, -y_p, q_p^2)$, as well as $F_e(x_p, y_p, q_p^2)$, which is $\eta_\gamma \rightarrow 0$ limit of $\bar{\Gamma}_e(x_p, y_p, q_p^2)$, will always be greater than or equal to zero inside the physical region. On the other hand, $\bar{\Gamma}_o(x_p, y_p, q_p^2)$, which is proportional to subtraction of two positive quantities, as well as $F_o(x_p, y_p, q_p^2)$, which is $\eta_\gamma \rightarrow 0$ limit of $\bar{\Gamma}_o(x_p, y_p, q_p^2)$, could be positive, zero or negative inside the allowed region.

We now define an observable, R_η , as

$$R_\eta(x_p, y_p, q_p^2) = \frac{\bar{\Gamma}_o}{\bar{\Gamma}_e} \approx \frac{F_o}{F_e} \left[1 + \eta_\gamma \left(\frac{G_o}{F_o} - \frac{G_e}{F_e} \right) \right] \quad (18)$$

and the asymmetry, $A_\eta(x_p, y_p, q_p^2)$, in R_η as

$$A_\eta(x_p, y_p, q_p^2) = \left(\frac{R_\eta}{R_{\text{SM}}} - 1 \right) \approx \eta_\gamma \left(\frac{G_o}{F_o} - \frac{G_e}{F_e} \right) \quad (19)$$

where,

$$R_{\text{SM}} = \frac{\bar{\Gamma}_o}{\bar{\Gamma}_e} \Big|_{\eta_\gamma=0} = \frac{F_o}{F_e}.$$

Since, F_o and G_o are the zeroth order and first order terms respectively in the expansion of the odd part of $\bar{\Gamma}(x_p, y_p, q_p^2)$ with respect to η_γ (see Eq. (16)), both of them are expected to be proportional to odd powers of y_p , rendering the ratio (G_o/F_o) to be finite at $y_p = 0$.

We will now show that F_o i.e. the odd part of SM, has a zero for this mode for all q_p^2 . For simplicity, to describe the situation mathematically, we consider only the dominant contributions arising from the first and second Feynman diagrams in Fig. 1. Retaining only relevant terms upto $\mathcal{O}(1/m_W^4)$, we can write,

$$F_o \propto y_p h(x_p, y_p, q_p^2) f(x_p, y_p, q_p^2) \quad (20)$$

where,

$$h = \left[\frac{1 + q_p^2}{(1 - q_p^2)^5 (1 - 2x_p) \{(1 - q_p^2 - x_p)^2 - y_p^2\}^2} \right], \quad (21)$$

$$\begin{aligned} f = & \left[7q_p^8 - 4(4 - x_p)q_p^6 + (11 - 4x_p + 6x_p^2 - 6y_p^2) \right. \\ & q_p^4 - 2q_p^2(1 - x_p + 8x_p^2 - 6x_p^3 - 4y_p^2 + 2x_py_p^2) \\ & + 3x_p^4 - 12x_p^3 + x_p^2(11 - 2y_p^2) - x_p(2 - 4y_p^2) \\ & \left. - y_p^2(3 + y_p^2) \right]. \end{aligned} \quad (22)$$

As can be seen from the inequalities in Eq. (15), $h(x_p, y_p, q_p^2)$ is always positive inside the physical region. Hence, the deciding factor on the sign of F_o is only $f(x_p, y_p, q_p^2)$. Now, on $x_p = 1/2$ surface, we have

$$f\left(\frac{1}{2}, y_p, q_p^2\right) = \frac{7}{16}(1 - 2q_p^2)^4 - \frac{3}{2}(1 - 2q_p^2)^2 y_p^2 - y_p^4,$$

which after using the upper limit of $|y_p|$ from Eq. (15), implies that

$$f\left(\frac{1}{2}, y_p, q_p^2\right) \geq 0, \quad (23)$$

$$\implies F_o\left(\frac{1}{2}, |y_p|, q_p^2\right) \geq 0, \quad (24)$$

$$F_o\left(\frac{1}{2}, -|y_p|, q_p^2\right) \leq 0. \quad (25)$$

Similarly for any point on the curved surface $(q_p^4 - q_p^2 + x_p^2 - y_p^2) = 0$ denoted as C , we have $y_p^2 = (q_p^4 - q_p^2 + x_p^2)$ and hence,

$$f(x_p, y_p, q_p^2) \Big|_C = (1 - q_p^2)(1 - 2x_p)^2(q_p^2 - 2x_p). \quad (26)$$

On using the limits of x_p and q_p^2 from Eq. (15), it can easily be shown that

$$f(x_p, y_p, q_p^2) \Big|_C \leq 0, \quad (27)$$

$$\Rightarrow F_o(x_p, |y_p|, q_p^2) \Big|_C \leq 0, \quad (28)$$

$$F_o(x_p, -|y_p|, q_p^2) \Big|_C \geq 0. \quad (29)$$

We have concluded that $f(x_p, y_p, q_p^2) < 0$ along the curve

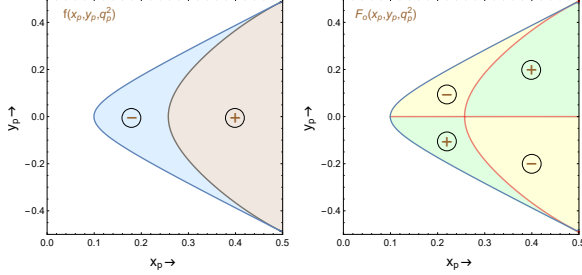


FIG. 3. The variations of functions $f(x_p, y_p, q_p^2)$ and $F_o(x_p, y_p, q_p^2)$ are shown in x_p - y_p plane in left and right panel, respectively, where $q_p^2 = 0.01$. The blue line in both the panels indicates one boundary of phase space with $\cos\theta = -1$ or $(q_p^4 - q_p^2 + x_p^2 - y_p^2) = 0$. In the left panel, the blue region signifies negative valued $f(x_p, y_p, q_p^2)$, the brown region symbolizes positive valued $f(x_p, y_p, q_p^2)$ and the black curve indicates $f(x_p, y_p, q_p^2) = 0$. In the right panel, the yellow region signifies negative valued $F_o(x_p, y_p, q_p^2)$, the green region symbolizes positive valued $F_o(x_p, y_p, q_p^2)$ and the red curve indicates $F_o(x_p, y_p, q_p^2) = 0$.

C and $f(x_p, y_p, q_p^2) > 0$ at the other boundary surface $x_p = 1/2$. It is obvious therefore that there must be at least one surface within the allowed phase space region where $f(x_p, y_p, q_p^2) = 0$. In the first plot of Fig. 3, the blue region signifies $f(x_p, y_p, q_p^2) < 0$ and the brown region symbolizes $f(x_p, y_p, q_p^2) > 0$ whereas the black curve indicates $f(x_p, y_p, q_p^2) = 0$. In the second plot of Fig. 3, the yellow region signifies $F_o(x_p, y_p, q_p^2) < 0$ and the green region symbolizes $F_o(x_p, y_p, q_p^2) > 0$ while the red curve indicates $F_o(x_p, y_p, q_p^2) = 0$.

The odd ($\bar{\Gamma}_o$) and even ($\bar{\Gamma}_e$) parts of differential rate as well as the four functions F_o, F_e, G_o, G_e contain soft collinear divergences arising due to $E_\gamma = 0$ or $\cos\theta = 1$ and divergence due to vanishing E_e if m_e is ignored. It is obvious from Eq. (12) that soft photon dominate in the region corresponding to $(x_p + y_p) \approx (1 - q_p^2)$, which implies $(x_p + y_p)$ is close to its maximum value. Hence, events with small photon energy lie at the top corner in Fig. 3 where the blue curve meets $x_p = 1/2$ line. Similarly, one can see from Eq. (11) that small electron energy implies $(x_p - y_p) \approx (1 - q_p^2)$ and these events lie at the bottom corner in Fig. 3 where the blue curve meets $x_p = 1/2$ line. For any value of q_p^2 , the collinear divergence occurs along $x_p = 1/2$ line as can easily be seen from Eq. (13). These singularities are evident from Eq. (21) and occur

in each of $\bar{\Gamma}, \bar{\Gamma}_o, \bar{\Gamma}_e$ as well as the four functions F_o, F_e, G_o, G_e . It is only in these regions that an expansion in powers of m_e/m_μ is not valid; the electron mass needs to be retained and ignoring it alters the differential decay rates. To deal with the $x_p = 1/2$ collinear singularity we choose an appropriate cut on x_p which is also necessitated by experimental resolution. It can be seen from Eq. (19), however, that with in SM, A_η is finite and zero, even in the regions plagued by collinear soft photon singularities and the ones that arise due to neglect of m_e . Note, that in A_η the h -function in Eq. (21) carrying the singular denominator cancels. The zero observed in F_o and the consequent singularity in the asymmetry A_η has nothing to do with the well know collinear soft photon and $m_e \rightarrow 0$ singularities. The zero observed in F_o is genuine and looks like an apparent exchange symmetry between E_e and E_γ only for the appropriately chosen parameters, x_p and y_p (or x_n and y_n defined in Eq. (A6)) with m_e retained.

We have explicitly demonstrated that there exists a surface (besides $y_p = 0$ plane) where $F_o(x_p, y_p, q_p^2) = 0$; we refer to this surface corresponding to the ‘new type of zero’ as ‘null-surface’. This means that at each point on this surface the differential decay rate $\bar{\Gamma}(x_p, y_p, q_p^2)$ remains unaltered if we interchange the energies of photon and electron. Hence, $A_\eta(x_p, y_p, q_p^2)$ diverges on null-surface for any non-zero value of η_γ and becomes zero everywhere in the phase space for η_γ being zero. The null-surface divides the phase space into two regions, one where A_η is positive and the other where A_η is negative. For $\eta_\gamma > 0$, $A_\eta < 0$ for x_p values smaller than the values indicated by the null-surface, whereas, $A_\eta > 0$ for x_p values larger than the values indicated by the null-surface. However, if $\eta_\gamma < 0$, an opposite behaviour in the signs of A_η is indicated. This feature can be used to determine the sign of η_γ . To measure the value of η_γ experimentally, one must average A_η over specified regions of phase space where it could be positive or negative. Such averages are necessitated by the experimental resolutions for q_p^2, x_p and y_p and will in general reduce the asymmetry. Hence, it is convenient to use $|A_\eta|$ as the asymmetry.

In the next section (Sec. IV) we probe the feasibility to measure η_γ using the asymmetry obtained in this section.

IV. SIMULATION AND ANALYSIS

In order to study the sensitivity of muon radiative decay mode we need to include the resolutions for energy of photon, energy of electron and the angle between them. We take them to be 2%, 0.5% and 10 Milli-radian, respectively [20]. As can be seen from Eq. (11)-(13), the resolutions for x_p, y_p and q_p^2 will also vary at different point in phase space due to the functional form of these parameters. We begin by evaluating the resolutions for x_p, y_p and q_p^2 for the entire allowed phase space. We find that the resolutions for x_p, y_p and q_p^2 are always less than 0.01, 0.02 and 0.02 respectively. For simplicity, in our simula-

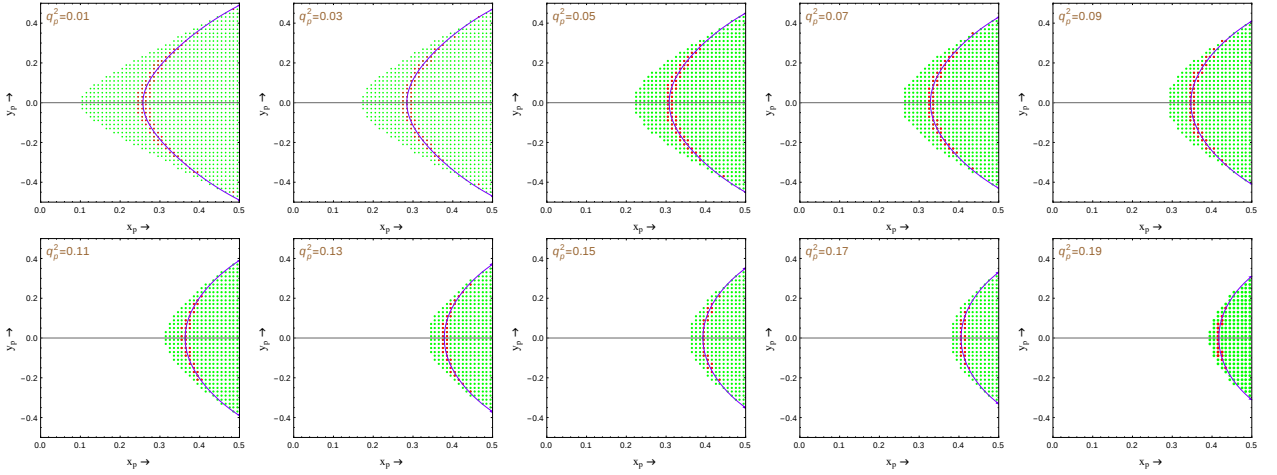


FIG. 4. The variation of $F_o(x_p, y_p, q_p^2)$ for different q_p^2 in the x_p - y_p plane. Each green dot represents a bin according to experimental resolution of photon energy, electron energy and angle between them. The red dots stand for the bins having $\delta|A_\eta|/|A_\eta| \leq 10$ in that bin. The purple curve signifies $F_o = 0$ in different q_p^2 plane. Our numerical analysis includes the bins corresponding to the red dots only. This results in an optimal sensitivity to η_γ .

tion, we take the worst possible scenario and assume constant resolutions for each of x_p , y_p and q_p^2 , corresponding to their largest value of 0.01, 0.02 and 0.02 respectively throughout the entire allowed phase space, which allows us to choose equal size bins. Hence, the phase space region $0 \leq q_p^2 \leq 1/2$, $0 \leq x_p \leq 1/2$, $-1/2 \leq y_p \leq 1/2$ is divided into 25 bins in q_p^2 and 50 bins in both x_p and y_p – all equal in size. Among these bins, only 6378 number of bins lie inside the physical phase space region. We next estimate the systematic and statistical error for $|A_\eta|$ in each of these bins, assuming $\eta_\gamma = 0.01$.

To find the systematic error in $|A_\eta|$ for a particular i -th bin, we evaluate it at 62,500 equally spaced points in that bin to estimate $|A_\eta|_i^j$ where j is the index of a point inside the i -th bin. However, for the bins near to the boundary of phase space, all of these points will not be inside the physical region and hence, we denote the number of physical points inside i -th bin as n_i . We now, calculate the average of $|A_\eta|_i^j$ inside a bin, i.e.

$$\langle |A_\eta|_i \rangle = \frac{1}{n_i} \sum_j |A_\eta|_i^j,$$

and take this as the asymmetry of that bin. Then we take the systematic error as the average deviation of $|A_\eta|_i^j$, i.e.

$$\sigma_i^{\text{sys}} = \frac{1}{n_i} \sum_j | \langle |A_\eta|_i \rangle - |A_\eta|_i^j |.$$

Ideally the errors can and should have been calculated using a standard Monte-Carlo technique with more number of sample points. The approach followed in this paper is to express the integral as a Riemann sum only for simplicity.

The statistical error for $|A_\eta|$ in each bin is also estimated by averaging it at the same 62,500 equally spaced

points. Note that, while A_η is divergent on the null-surface the average value of $|A_\eta|$ for the i -th bin, i.e. $\langle |A_\eta|_i \rangle$, estimated from Monte Carlo studies is never larger than 10^{-6} for any bin. Hence,

$$\sigma_i^{\text{sta}} = \sqrt{\frac{1 - \langle |A_\eta|_i \rangle^2}{N_i}} \approx \frac{1}{\sqrt{(N_{SM})_i}},$$

where i is the index of the bins and N_i represents the number of events inside i -th bin which is almost the same as $(N_{SM})_i$ the number of SM events for the i -th bin. We have also assumed that both A_η and the effects of η_γ on N_i are small and can be ignored. If this were not the case N_i would itself be sensitive to η_γ , contrary to our simulation results. Hence, we simply take the statistical error for all practical purposes to be that in the case of SM events. The number of events in each bin is calculated by taking total number of muons to be 10^{19} . To avoid the singularities in the number of SM events for the bins near $x_p = 1/2$ plane, we ignore the bins with $0.49 \leq x_p \leq 0.5$.

The total error in $|A_\eta|$ for any particular bin is then given by $\delta|A_\eta|_i = \sqrt{(\sigma_i^{\text{sta}})^2 + (\sigma_i^{\text{sys}})^2}$. This error in $|A_\eta|$ will affect the measurement of η_γ . Using Eq. (19), we observe that the error in the measurement of η_γ in each bin as

$$\left| \frac{\delta\eta_\gamma}{\eta_\gamma} \right|_i = \frac{\delta|A_\eta|_i}{|A_\eta|_i} \quad (30)$$

where, $|A_\eta|_i \equiv \langle |A_\eta|_i \rangle$ and we take the theoretical function $(G_o/F_o - G_e/F_e)$ to be free from experimental uncertainties. It is obvious from Eq. (30), that the highest sensitivity is achieved in bins close to the null-surface where $|A_\eta|_i$ is the largest. Hence, we consider only the region along the null-surface by applying a cut $\delta|A_\eta|_i/|A_\eta|_i \leq 10$ to determine η_γ .

In Fig. 4, we depict the bins, which satisfy the above cut, with red dots for different q_p^2 values, whereas, the green dots signify all the other bins inside the physical region; the purple curve indicates the null-surface where $F_o = 0$ for the corresponding q_p^2 value. Including only the bins, which satisfy the above cut, for a simulated value of $\eta_\gamma = 0.01$ (at one loop in SM, $|\eta_\gamma| \lesssim 0.015$), we estimate an error of $\delta\eta_\gamma = 2.6 \times 10^{-3}$, implying a 3.9σ significance for the measurement. A total of 10^{19} muons are aimed for in the long term future. The next-round of experiments are aiming at 10^{18} muons /year. This reduces the sensitivity from 3.9σ to 1.4σ . To appreciate the advantage of radiative muon decays in measuring $WW\gamma$ vertex one needs to note that the current global average of κ_γ differs from unity only by 0.4σ . We note that the significance of the measured value of η_γ may in principle be improved by optimizing the chosen cut and binning procedure. However, we refrain from such intricacies as our approach is merely to present a proof of principle.

We have shown that the sensitivity to η_γ arises due to the vanishing of the odd differential decay rate in the standard model denoted by F_o . The observed singularity in A_η is unrelated to soft photon and collinear singularities or the singularity arising due to neglect of m_e in calculations. The most sensitive region to measure η_γ is where A_η is large and obviously lies along the zero of F_o as indicated by Eq. (19). The region around $F_o = 0$ for which $\delta|A_\eta|_i/|A_\eta|_i \leq 10$, is where a legitimate expansion in powers of m_e/m_μ can be carried out and is distinct from the singular regions in the differential decay rates where such an expansion cannot be done. However, in order to verify the accuracy of sensitivity achievable in η_γ measurement the calculations have been redone by numerically retaining m_e . We find that for the bins represented by red dots in Fig. 4 the maximum correction in η_γ is $\mathcal{O}(10^{-4})$, which is an order of magnitude smaller than the error in it, $\delta\eta_\gamma = 2.6 \times 10^{-3}$.

Finally, we discuss possible sources of inaccuracies in our estimation of uncertainty. Higher order electroweak corrections to the process considered will modify the decay rate and alter F_o . While higher order electroweak corrections have not been included in our analysis they have been worked out in detail [21]. However, this is unlikely to affect our analysis technique as we have selected bins to be included in estimating η_γ purely based on the criterion $\delta|A_\eta|_i/|A_\eta|_i \leq 10$ and not on the location and validity of the null-surface. A possible source of uncertainty that we have ignored in our analysis is the assumption that the muon decays at rest or with known four-momenta. While facilities that produce large numbers of muons are designed to bring the muon to rest, a fraction of them may decay with a finite but unknown 4-momenta, rendering the exact measurement of q_p^2 inaccurate. This effect can in-principle be considered by including additional systematic errors in q_p^2 .

V. CONCLUSION

In order to probe lepton flavor violating process $\mu \rightarrow e\gamma$, facilities that produce large numbers of muons are being designed. We show that radiative muon decay $\mu \rightarrow e\gamma\nu_\mu\bar{\nu}_e$ is a promising mode to probe loop level corrections in the SM to the C and P conserving dimension four $WW\gamma$ vertex with good accuracy. The process has two missing neutrinos in the final state and on integrating their momenta the partial differential decay rate removes the well known radiation-amplitude-zero. We show, however, that the normalized differential decay rate, odd under the exchange of photon and electron energies, does have a zero in the case of standard model (SM). This *new type of zero* had hitherto not been studied in literature. A suitably constructed asymmetry using this fact enables a sensitive probe for the $WW\gamma$ vertex beyond the SM. The large number of muons produced keeps the statistical error in control for a tiny part of the physical phase space, enabling us to measure $\eta_\gamma = 0.01$ with 3.9σ significance.

ACKNOWLEDGMENTS

We thank Yoshitaka Kuno, Marcin Chrzaszcz, Thomas G. Rizzo and Jernej F. Kamenik for valuable suggestions and discussions. The work of RM is supported in part by Grants No. FPA2014-53631-C2-1-P, FPA2017-84445-P and SEV-2014-0398 (AEI/ERDF, EU) and by PROM-ETEO/2017/053.

Appendix A: Expressions with electron mass retained

In presence of electron mass m_e , we have $s + t + u = q^2 + m_\mu^2 + m_e^2$ where the Mandelstam variables are defined as: $(p_e + p_\gamma)^2 = s$, $(p_e + q)^2 = t$ and $(p_\gamma + q)^2 = u$. The physical region is determined by the following inequalities [22]:

$$m_e^2 \leq s \leq (m_\mu - \sqrt{q^2})^2, \quad (\text{A1})$$

$$q^2 \leq u \leq (m_\mu - m_e)^2, \quad (\text{A2})$$

$$(m_e + \sqrt{q^2})^2 \leq t \leq m_\mu^2, \quad (\text{A3})$$

$$G[s, u, m_\mu^2, 0, m_e^2, q^2] \leq 0. \quad (\text{A4})$$

where

$$G[x, y, z, u, v, w] = -\frac{1}{2} \begin{vmatrix} 0 & 1 & 1 & 1 & 1 \\ 1 & 0 & v & x & z \\ 1 & v & 0 & u & y \\ 1 & x & u & 0 & w \\ 1 & z & y & w & 0 \end{vmatrix} \quad (\text{A5})$$

We define variables x_n, y_n and q_n^2 , which reduce to

x_p, y_p and q_p^2 at $m_e \rightarrow 0$ limit, in the following way:

$$\begin{aligned} x_n &= \frac{t+u}{2(q^2 + m_\mu^2 + m_e^2)}, \\ y_n &= \frac{t-u+m_e^2}{2(q^2 + m_\mu^2 + m_e^2)}, \\ q_n^2 &= \frac{q^2}{(q^2 + m_\mu^2 + m_e^2)}, \end{aligned} \quad (\text{A6})$$

The energy of electron and photon are obtained from the above definitions as:

$$E_e = \frac{(2m_\mu^2 + m_e^2)(1 - q_n^2 - x_n + y_n) - m_e^2(x_n - y_n)}{4m_\mu(1 - q_n^2)}, \quad (\text{A7})$$

$$E_\gamma = \frac{(2m_\mu^2 + m_e^2)(1 - q_n^2 - x_n - y_n) - m_e^2(x_n + y_n)}{4m_\mu(1 - q_n^2)}. \quad (\text{A8})$$

Under the replacement $y_n \rightarrow -y_n$ electron and photon energies get exchanged and one separate the odd and even parts differential decay rate as follows:

$$\begin{aligned} \bar{\Gamma}_o(x_n, y_n, q_n^2) &= \frac{1}{2} [\bar{\Gamma}(x_n, y_n, q_n^2) - \bar{\Gamma}(x_n, -y_n, q_n^2)] \\ \bar{\Gamma}_e(x_n, y_n, q_n^2) &= \frac{1}{2} [\bar{\Gamma}(x_n, y_n, q_n^2) + \bar{\Gamma}(x_n, -y_n, q_n^2)] \end{aligned} \quad (\text{A9})$$

The h -function in Eq. (21) containing singular denominator, now, becomes

$$h \propto \frac{1}{E_e^2 E_\gamma^2 (m_\mu^2(1 - 2x_n) + m_e^2(q_n^2 - 2x_n))}. \quad (\text{A10})$$

The region around $F_o = 0$ which are denoted by red dots in Fig. 4, a legitimate expansion in powers of (m_e/m_μ) for the expressions of $\bar{\Gamma}_o$ and $\bar{\Gamma}_e$ can be carried out in the following way:

$$\bar{\Gamma}_o \approx (F_o + (m_e/m_\mu)^2 \delta F_o) + \eta_\gamma (G_o + (m_e/m_\mu)^2 \delta G_o) \quad (\text{A11})$$

$$\bar{\Gamma}_e \approx (F_e + (m_e/m_\mu)^2 \delta F_e) + \eta_\gamma (G_e + (m_e/m_\mu)^2 \delta G_e) \quad (\text{A12})$$

where the small η_γ^2 terms are ignored. Here, δF_o , δG_o , δF_e and δG_e are the leading order correction terms due to non zero electron mass. The observable R_η , now, gets modified as:

$$\begin{aligned} R_\eta(x_n, y_n, q_n^2) &= \frac{\bar{\Gamma}_o(x_n, y_n, q_n^2)}{\bar{\Gamma}_e(x_n, y_n, q_n^2)} \\ &\approx \left(\frac{F_o + (\frac{m_e}{m_\mu})^2 \delta F_o}{F_e + (\frac{m_e}{m_\mu})^2 \delta F_e} \right) \\ &\times \left[1 + \eta_\gamma \left(\frac{G_o + (\frac{m_e}{m_\mu})^2 \delta G_o}{F_o + (\frac{m_e}{m_\mu})^2 \delta F_o} - \frac{G_e + (\frac{m_e}{m_\mu})^2 \delta G_e}{F_e + (\frac{m_e}{m_\mu})^2 \delta F_e} \right) \right] \end{aligned} \quad (\text{A13})$$

Hence, the asymmetry, $A_\eta(x_p, y_p, q_p^2)$, in R_η becomes,

$$\begin{aligned} A_\eta(x_n, y_n, q_n^2) &= \left(\frac{R_\eta}{R_{\text{SM}}} - 1 \right) \\ &\approx \eta_\gamma \left(\frac{G_o + (\frac{m_e}{m_\mu})^2 \delta G_o}{F_o + (\frac{m_e}{m_\mu})^2 \delta F_o} - \frac{G_e + (\frac{m_e}{m_\mu})^2 \delta G_e}{F_e + (\frac{m_e}{m_\mu})^2 \delta F_e} \right) \\ &\approx \eta_\gamma \left(\frac{G_o}{F_o} - \frac{G_e}{F_e} \right) \\ &\quad + \eta_\gamma \left(\frac{m_e}{m_\mu} \right)^2 \left(\frac{G_e \delta F_e}{F_e^2} - \frac{G_o \delta F_o}{F_o^2} + \frac{\delta G_o}{F_o} - \frac{\delta G_e}{F_e} \right) \end{aligned} \quad (\text{A14})$$

where,

$$R_{\text{SM}} = \frac{\bar{\Gamma}_o}{\bar{\Gamma}_e} \Big|_{\eta_\gamma=0} = \left(\frac{F_o + (\frac{m_e}{m_\mu})^2 \delta F_o}{F_e + (\frac{m_e}{m_\mu})^2 \delta F_e} \right).$$

Note that the above expansion in $\mathcal{O}(m_e/m_\mu)$ fails in the region where collinear or soft photon divergences occurs.

-
- [1] S. Chatrchyan et al. (CMS Collaboration), Phys. Rev. D 89, 092005(2014)
 - [2] G. Aad et al. (ATLAS Collaboration), Phys. Rev. D 87, 112003(2013)
 - [3] Victor Mukhamedovich Abazov et al. (D0 Collaboration), Phys. Lett. B 718 (2012) 451-459
 - [4] T. Aaltonen et al. (CDF Collaboration), Phys. Rev. Lett. 104 (2010) 201801
 - [5] J. Abdallah et al. (DELPHI Collaboration), Eur. Phys. J. C 66 (2010) 35-56
 - [6] S. Schael et al. (ALEPH Collaboration), Phys. Lett. B 614 (2005) 7-26
 - [7] G. Abbiendi et al. (PAL Collaboration), Eur. Phys. J. C 33 (2004) 463-476
 - [8] P. Achard et al. (L3 Collaboration), Phys. Lett. B 586 (2004) 151-166
 - [9] G. Couture and J. N. Ng, Z. Phys. C 35, 65 (1987).
 - [10] C. Patrignani *et al.* [Particle Data Group], Chin. Phys. C 40, no. 10, 100001 (2016).
 - [11] K. O. Mikaelian, M. A. Samuel and D. Sahdev, Phys. Rev. Lett. 43, 746 (1979).
 - [12] COMET collaboration: <http://comet.kek.jp/>
 - [13] MEG collaboration: <https://meg.web.psi.ch/>
 - [14] Mu2e collaboration: <http://mu2e.fnal.gov/public/hep/general/proposals.shtml>
 - [15] Y. Kuno, Y. Okada, Rev. Mod. Phys. 73 (2001) 151-202
 - [16] K. Hagiwara, R.D. Peccei and D. Zeppenfeld, Nucl. Phys. B282, 253 (1987).
 - [17] W. J. Marciano and A. Queijeiro, Phys. Rev. D 33, 3449 (1986).
 - [18] L. M. Sehgal, Phys. Lett. B 569, 25 (2003)
 - [19] V. S. Schulz and L. M. Sehgal, Phys. Lett. B 594, 153 (2004).
 - [20] Private communication with Yoshitaka Kuno.
 - [21] A.B. Arbuzov, E.S. Scherbakova, Phys. Lett. B 597 (2004) 285-290; M. Fael, L. Mercolli, M. Passera, Phys. Rev. D 88 (2013) no.9, 093011; M. Fael, L. Mercolli, M. Passera, JHEP 1507 (2015) 153; G. M. Pruna, A. Signer,

Y. Ulrich, Phys. Lett. B 772 (2017) 452-458

[22] Particle Kinematics by E. Byckling & K. Kajantie, page 106-107